Eng. Sci., 2020, 11, 36-43

Engineered Science

DOI: https://dx.doi.org/10.30919/es5e1006

Facile Synthesis of $LiMn_{0.75}Fe_{0.25}PO_4$/C Nanocomposite Cathode Materials of Lithium-Ion Batteries through Microwave Sintering

Chunping Hou,[1,2] Jiao Hou,[3] Hao Zhang,[1] Yong Ma,[1,4,*] Xiaowei He,[1] Wangchang Geng,[1] and Qiuyu Zhang[1,*]

Abstract

$LiMn_{0.75}Fe_{0.25}PO_4$/C nanocomposites are synthesized by a facile hydrothermal and ball-milling method, combining with spray-drying and microwave sintering process. X-ray diffractometer (XRD) and scanning electron microscopy (SEM) results reveal that the sintering process has a strong effect on the structures and morphologies of the as-prepared powders, and thus on the subsequent electrochemical performance. The lattice parameters (a, b, and c) of the microwave sintered sample are all smaller than those of the ordinary sintered sample. Meanwhile, compared to 299.66 $Å^3$ of unit cell volume for the ordinary heating sintered sample, the value of the microwave sintered sample is 299.15 $Å^3$. Transmission electron microscope (TEM) displays that the grains of the microwave sintered sample are less than 50 nm. The microwave sintered sample presents an excellent electrochemical performance with a discharge capacity of 143.5 mAh g^{-1} and capacity retention of 94.3% after 225 cycles at a rate of 0.1 C. Cyclic voltammetry (CV) and electrochemical impedance spectroscopy (EIS) show that the microwave sintered electrode has a smaller charge-transfer resistance and a minor polarization and thus results in improved electrode kinetics. The microwave sintering is an economic, energy-saving, and time-saving synthetic method, which has great industrial application prospects.

Keywords: Li-ion batteries; Cathode material; Microwave sintering; Lattice parameters; Electrochemical performance.
Received: 9 February 2020; Accepted: 21 April 2020.
Article type: Research article.

1. Introduction

Since Padhi's first report,[1] lithium manganese phosphate ($LiMnPO_4$) has been considered as a promising cathode material for Li-ion batteries due to its lower cost, abundant source, environmental compatibility, good thermal stability, and long cycle life, especially for the uses of electric or hybrid electric vehicles, and dispersed energy storage.[2-10] In comparison with lithium iron phosphate ($LiFePO_4$), lithium manganese phosphate ($LiMnPO_4$) possesses a higher redox potential (4.1 V vs. Li/Li^+) and larger theoretical energy density (701 Wh kg^{-1}). Furthermore, $LiMnPO_4$ is well compatible with the currently used electrolytes for 4 V positive electrodes such as lithium cobalt oxide ($LiCoO_2$) and lithium manganese oxide ($LiMn_2O_4$) cathodes. However, $LiMnPO_4$ suffers from low electronic conductivity ($<10^{-10}$ S cm^{-1}),[11-13] low Li^+ diffusion coefficient,[14,15] local structure distortion caused by Jahn-Teller effect of active Mn^{3+} ions[16] and a large cell volume change between $LiMnPO_4$ and $MnPO_4$ during the charge/discharge process.[17,18] To overcome these shortcomings, different strategies have been adopted to optimize the properties of $LiMnPO_4$ by using nanoscale particles,[19] doping,[20-22] carbon coating,[23,24] conductive additive loading,[25] and various synthesis techniques.[26-31] Thereinto, Fe substitution has been proved to be more effective to improve the electrochemical characteristics of $LiMnPO_4$ cathode material and is promising for large-scale applications.[23,32] It can dramatically improve Li^+ and electron transport in the bulk and charge transfer on the surface of the nanocrystals.[33]

Although the common solid-phase synthesis has many advantages, such as simple process and low cost, the electrochemical properties of the prepared material are poor. Compared to solid-phase synthesis, the materials fabricated by

[1]*Key Laboratory of Special Functional and Smart Polymer Materials of Ministry of Industry and Information Technology, Northwestern Polytechnical University, Xi'an Shanxi, 710129, China.*
[2]*College of Materials Science and Engineering, North Minzu University, Yinchuan Ningxia, 750021, China.*
[3] *College of Chemistry and Chemical Engineering, North Minzu University, Yinchuan Ningxia, 750021, China.*
[4]*School of Material Science and Engineering, Shandong University of Science and Technology, Qingdao Shandong, 266590, China.*
**E-mail: courage2010@126.com (Y. Ma); qyzhang@nwpu.edu.cn (Q. Zhang).*

liquid-phase synthesis possess good electrochemical performances. However, much more complicated synthesis processes and higher energy consumption lead to some limitations in practice. Therefore, it is necessary to consider a facile synthesis method to prepare $LiMnPO_4$ with better electrochemical performances and energy-saving spontaneously, which is also a low cost and time-saving synthetic method with great industrial application prospects.

Liquid-phase synthesis, such as hydrothermal, sol-gel, solvothermal, polyol, can make the material's particles in a refined nanoscale. Recently, composite materials based on $LiMnPO_4$ have been obtained and exhibited significant performances with the combination of liquid-phase synthesis and conventional technologies. For example, Wu *et al.*[34] prepared $LiMnPO_4$/C cathode materials by a sol-gel method combined ball milling and liquid nitrogen quenching method. It is revealed that quenching inhibited the growth and agglomeration of $LiMnPO_4$/C particles and resulted in the formation of defects in $LiMnPO_4$ crystals, therefore greatly improving the electrochemical performance of $LiMnPO_4$/C. Microwave-assisted synthesis is taken as an energy-saving and fast synthesis method for the electrode materials. For example, Kim *et al.*[35] synthesized $LiMn_{0.75}Fe_{0.25}PO_4$/C microspheres through using a microwave-assisted process with a complexing agent, and found that the prepared product had a high tap density of 1.3 g cm^{-3} and delivered a reversible capacity of 163 mAh g^{-1} at a 0.05 C-rate. Furthermore, 57% capacity retention at a 60 C-rate as well as 99.3% capacity retention after 100 cycles at 1 C-rate were obtained. Yu *et al.*[36] adopted both condition-controlled microwave heating and conventional heating to synthesize $LiFePO_4$/C microspheres, respectively. It was found that the microwave heated $LiFePO_4$/C sample had a 3D porous structure with a particle size of about 20-30 nm, which exhibited higher capacities, excellent rate capability, and a better dynamic performance (higher Li^+ diffusion and lower polarization). Although the microwave-assisted method was frequently used in both hydrothermal synthesis and solvothermal synthesis for $LiMnPO_4$, there are few literatures about microwave heating sintered $LiMnPO_4$ cathode material. In this paper, the $LiMn_{0.75}Fe_{0.25}PO_4$/C powders were prepared by a facile hydrothermal and ball-milling method and then sintered by microwave heating. The improvement of the electrical conductivity and the enhancement of Li^+ diffusion for $LiMnPO_4$ cathode material were researched in detail.

2. Experimental section

2.1 Preparation of $LiMn_{0.75}Fe_{0.25}PO_4$/C composites

$LiMn_{0.75}Fe_{0.25}PO_4$ nanoparticles were synthesized by a facile hydrothermal method.[24] The as-prepared $LiMn_{0.75}Fe_{0.25}PO_4$ precursor was mixed with a sucrose solution in a 10:2 weight ratio, and the mixture was milled at 40 Hz for 24 h with a ball-to-material ratio of 10:1 (Shanghai Dingpai Mechanical Equipment Co., Ltd., 0.4 L). The slurry was spray dried on a GZ-5 spray dryer with an inlet temperature of 220 °C and an outlet temperature of 120 °C. Then, the spherical $LiMn_{0.75}Fe_{0.25}PO_4$/sucrose composite obtained by secondary granulation was heated to 350 °C at a rate of 2 °C min^{-1} and maintained for 4 h in an N_2-filled box furnace (KBF13Q). Afterward, the composite was raised to 550 °C at a rate of 2 °C min^{-1}, and sintered for 10 h, then naturally cooled down to room temperature and sieved through a 200 mesh to obtain the $LiMn_{0.75}Fe_{0.25}PO_4$/C nanoparticles (marked as contrast sample A). Meanwhile, the $LiMn_{0.75}Fe_{0.25}PO_4$/sucrose composite was treated with a MobileLab Microwave Station (4 kW, 2450 MHz (220 V)), heated to 350 °C at a rate of 10 °C min^{-1} and maintained for 2 h, and then heated to 550 °C and maintained for 5 h. Finally, the microwave sintered $LiMn_{0.75}Fe_{0.25}PO_4$/C nanoparticles were obtained (marked as sample B). The schematic illustration of the preparation process of $LiMn_{0.75}Fe_{0.25}PO_4$/C composites calcined by ordinary heating sintering and microwave sintering is exhibited in Scheme 1.

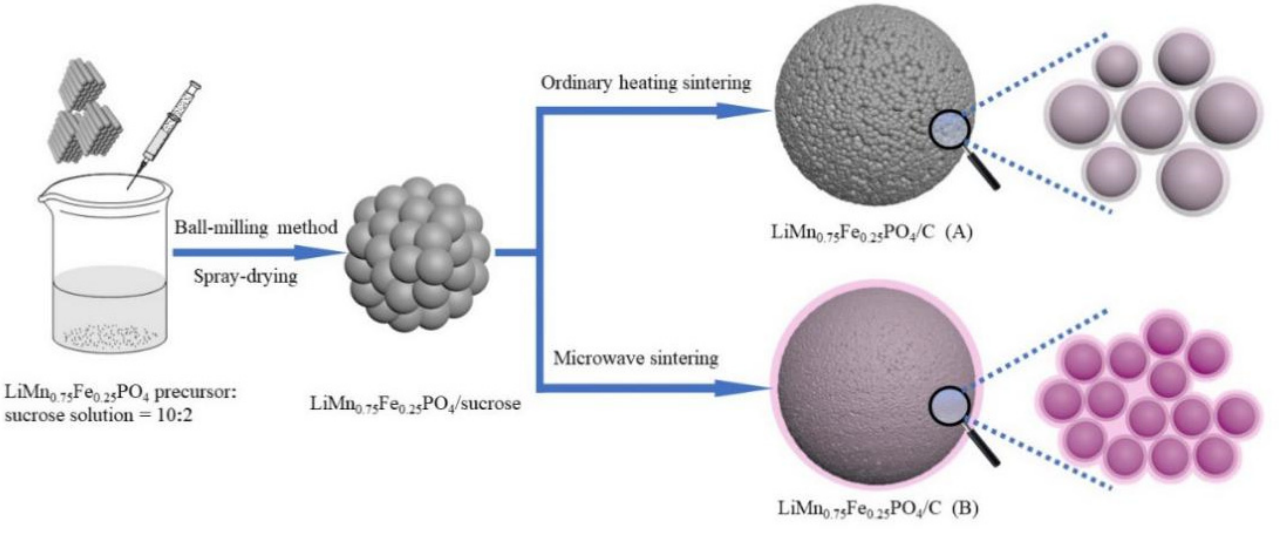

Scheme 1. The schematic illustration of the preparation process of $LiMn_{0.75}Fe_{0.25}PO_4$/C composites calcined by **(A)** ordinary heating sintering and **(B)** microwave sintering.

2.2 Characterization of $LiMn_{0.75}Fe_{0.25}PO_4/C$ composites

The crystal phases of the synthesized composite materials were characterized by an X-ray diffractometer (XRD) (XRD-7000S, Shimadzu, Japan) using Cu K_α radiation (λ=0.15423 nm) (40 kV 200 mA). The microscopic features of the samples were observed by field-emission scanning electron microscopy (SEM, JSM-6700F, JEOL, Japan) with an energy-dispersive X-ray spectroscopy (EDS) and a transmission electron microscopy (TEM, JEM-3010, JEOL, Japan). N_2 adsorption/desorption isotherms and specific areas were tested using a Tristar II surface area and porosity analyzer (Micromeritics Instruments Inc., USA).

2.3 Electrochemical measurements

The electrochemical properties of the samples were measured by assembling CR2025 coin cells. The composite electrodes were prepared by mixing $LiMn_{0.75}Fe_{0.25}PO_4/C$ composites with carbon black and polyvinylidene difluoride (PVDF) in a weight ratio of 85:8:7 in N-methyl pyrrolidone to form a homogeneous slurry. The slurry was coated on aluminum foil and dried in a vacuum oven at 120 °C for 12 h, then pressed and punched to disks. Finally, the cells were assembled in an Ar-filled glove box (LABSTAR 1250/750, MBRAUN, Germany) with lithium foil as the counter and the reference electrode, a polypropylene microporous film (Celgard 2400, USA) as the separator, and 1 M lithium hexafluorophosphate ($LiPF_6$) in ethylene carbonate (EC), diethyl carbonate (DEC), and dimethyl carbonate (FEC) (1:1:1, v/v/v) (LD-124B, Shanshan battery material Co., Ltd, China) as the electrolyte. The galvanostatic charge/discharge tests were conducted on a battery testing system (LAND CT2001A, Wuhan Jinnuo Electronics Co., Ltd., China) in the potential range of 2.5-4.5 V (vs. Li^+/Li) at rates of 0.1 and 0.2 C (1 C=171 mA g^{-1}). An electrochemical workstation (CHI660E, Shanghai Chenhua Instruments Inc., China) was used to perform the cyclic voltammetry tests by using a scan rate of 0.1 mV s^{-1} and a voltage range of 2.5-4.5 V (vs. Li^+/Li). The electrochemical impedance spectroscopy (EIS) was measured at room temperature. And the spectra were potentiostatically measured by applying an AC voltage of 5 mV from 10^5 to 10^{-2} Hz. All the tests were conducted at room temperature.

3. Results and discussion

As shown in Fig. 1, the XRD diffraction peaks of two samples are completely indexed to the orthorhombic Pnmb space group of $LiMnPO_4$ (PDF#740375) based on the olivine structure. The diffraction peaks of Fe-doped samples are slightly shifted to larger 2θ angles compared with those of pure $LiMnPO_4$ owing to the smaller ionic radius of Fe^{2+} doping homogeneously in a solid solution. The relative intensity of the diffraction peak of $LiMn_{0.75}Fe_{0.25}PO_4/C$ prepared by ordinary heating sintering is much higher than that of the sample prepared by microwave sintering. This case indicates that the former process makes the crystal growth more complete, the crystal structure more perfect and the defects much less due to the prolonged heating time. Of particular attention is that there are no characteristic peaks of crystal carbon observed in the patterns, demonstrating that the carbon in the composite is in the form of amorphous structure.

Sucrose is used as the carbon source to improve the electronic conductivity of the resulting product and inhibits the grain growth of $LiMn_{0.75}Fe_{0.25}PO_4$. The lattice parameters of $LiMn_{0.75}Fe_{0.25}PO_4/C$ prepared with different sintering ways by the Rietveld refinement method are listed in Table 1. The lattice parameters of a pure $LiMnPO_4$ are a=6.1000 Å, b=10.4600 Å, and c=4.7440 Å, which are larger than those listed in Table 1. This situation manifests that Fe partial substitution of Mn makes the cell volume shrink. Moreover, all the lattice parameters of the sample prepared by microwave sintering (a=6.0760 Å, b=10.4067 Å, and c=4.7310 Å) are smaller than those of one prepared by ordinary heating sintering (a=6.0774 Å, b=10.4149 Å, and c=4.7342 Å), and the cell volume also shrinks from 299.66 to 299.15 $Å^3$. Because of a faster heating rate, shorter sintering time and a quick cooling process, microwave sintering can suppress the grain growth. The effect is similar to the quenching process of $LiMnPO_4$ synthesis.

Table 1. Lattice parameters of $LiMn_{0.75}Fe_{0.25}PO_4/C$ composites calcined by ordinary heating sintering and microwave sintering.

Sample	A (Å)	b (Å)	C (Å)	Cell volume ($Å^3$)
Ordinary heating sintering	6.0774	10.4149	4.7342	299.66
Microwave sintering	6.0760	10.4067	4.7310	299.15

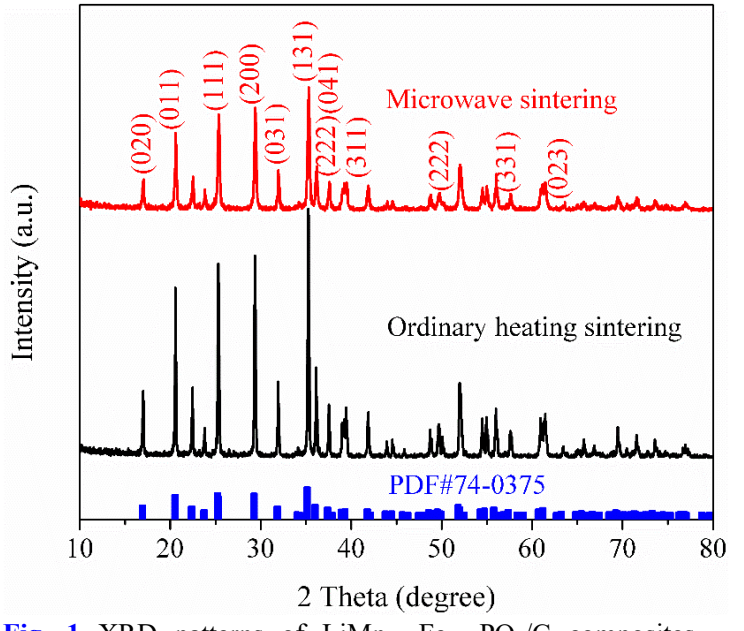

Fig. 1 XRD patterns of $LiMn_{0.75}Fe_{0.25}PO_4/C$ composites calcined by ordinary heating sintering and microwave sintering.

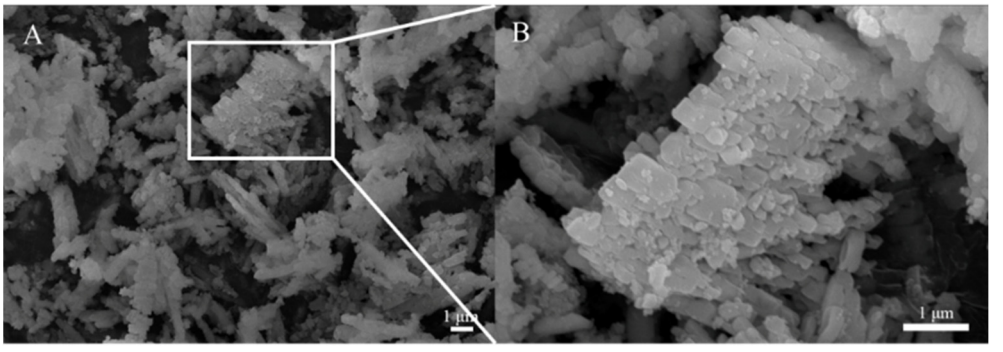

Fig. 2 SEM images of **(A)** $LiMn_{0.75}Fe_{0.25}PO_4$ precursor and **(B)** corresponding enlarged part.

Fig. 2A displays the SEM image of $LiMn_{0.75}Fe_{0.25}PO_4$ precursor and Fig. 2B is the corresponding enlarged image of the box area in Fig. 2A. It is found that the $LiMnPO_4$ precursor shows a rodlike shape with a diameter of about 200 nm and a length of about 1 μm and has an orientated array growth. The precursor structure is much bigger than that of the milled and sintered sample (about 50 nm).

The specific surface areas of the materials can be obtained by employing N_2 adsorption/desorption isotherms.[37-39] From Fig. 3 of N_2 adsorption/desorption isotherms, the specific surface areas of the $LiMn_{0.75}Fe_{0.25}PO_4/C$ composites obtained by ordinary heating sintering and microwave sintering are 20.227 and 21.212 $m^2\ g^{-1}$, respectively. The latter possesses a slightly larger specific surface area than the former. This fact is consistent with the variation trend of the lattice parameters measured by XRD. The microwave sintering process makes the heating rate increase faster and keeps a portion of carbon as stereochemical net structure, which results in the increment of the porosity and the specific surface area. Furthermore, microwave sintering inhibits the grain growth of the composites, followed by the formation of smaller particles and less agglomeration. This situation gives rise to a shorter Li^+ ion diffusion path and promotes electrochemical properties such as electronic conductivity.

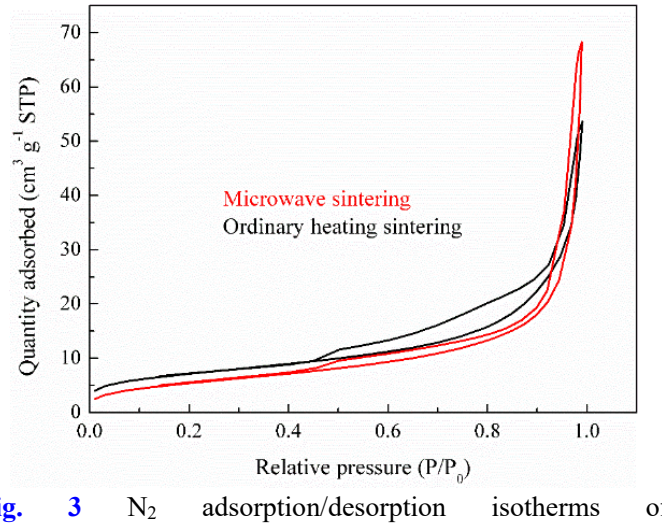

Fig. 3 N_2 adsorption/desorption isotherms of $LiMn_{0.75}Fe_{0.25}PO_4/C$ composites calcined by ordinary heating sintering and microwave sintering.

Fig. 4 shows the SEM images of the spray-drying $LiMn_{0.75}Fe_{0.25}PO_4/C$ composites which are in the shape of spherical aggregate particles. It is noteworthy that the surface morphologies of the microspheres prepared by different processes are remarkably different. In Fig. 4A1, the surface of the microspheres fabricated by ordinary heating sintering is rough, and the primary particles have not been distributed evenly in size. At a high magnification of Fig. 4A2, it is found that some sintered aggregates and primary particles are larger than 200 nm on the surface. However, there are two situations on the surface of microspheres prepared by microwave sintering: Fig. 4C presents a dense surface covering, and the size of uniformly distributed primary particles is about 100 nm; Fig. 4D shows no dense surface covering, but the size distribution of particles is more uniform than that of the ones prepared by ordinary heating sintering. EDS analyses in Table 2 exhibit that the carbon content of the area C is slightly higher than that of area D, implying that there may be a carbon shell structure. The existence of a carbon shell structure enhances the conductivity of the resulting composite. With respect to the composite obtained by ordinary heating, the size increase and the agglomeration of particles lead to the diffusion path increase and the Li^+ diffusion more difficult, thus reducing the conductivity of the composite.

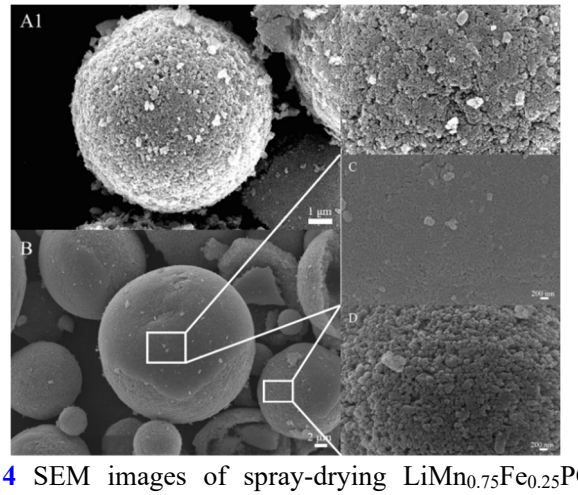

Fig. 4 SEM images of spray-drying $LiMn_{0.75}Fe_{0.25}PO_4/C$ composites calcined by **(A)** ordinary heating sintering and **(B)** microwave sintering, **(C) (D)** different enlarge parts of sample shown in (B).

Table 2. Phase compositions of area C and area D by using EDS semi-quantitative analyses.

Area	Composition (wt.%)					
	C	O	P	Mn	Fe	Total
C	16.39	35.35	17.92	22.38	7.96	100
D	15.58	36.06	17.85	22.47	8.04	100

Fig. 5A and 5B shows TEM images of primary particles and spherical aggregate particles of $LiMn_{0.75}Fe_{0.25}PO_4/C$ composite calcined by microwave sintering. Most of the particles are less than 50 nm, and the particle size distribution is relatively uniform. From the image, some hollow channels can be viewed. This particular structure enhances the Li^+ diffusion and contributes to improved electrochemical properties.

Fig. 6A and Fig. 6B respectively show the charge-discharge curves of $LiMn_{0.75}Fe_{0.25}PO_4/C$ composites calcined by ordinary heating sintering and microwave sintering measured in the range of 2.5-4.5 V at room temperature at different rates: 0.1 and 0.2 C. In the case of 0.1 C, the first discharge capacities of the two samples are 152.7 and 152.1 mAh g^{-1}, and the first coulombic efficiencies are 87.1% and 84.9 %, respectively. Both samples present two distinct charge plateaus curves and two distinct discharge plateaus curves, corresponding to the oxidation and reduction reactions of Mn^{3+}/Mn^{2+} and Fe^{3+}/Fe^{2+} during Li^+ deintercalation and intercalation for the $LiMn_{0.75}Fe_{0.25}PO_4/C$ composites. Nevertheless, the voltage difference of the main voltage platform of the ordinary heating sintered sample (0.24 V) is significantly larger than that of the microwave sintered sample (0.14 V), meaning that the electrode polarization of the latter is smaller than that of the former. The reason is that the microwave sintered sample has a finer particle size, which shortens the diffusion path of Li^+. This situation brings about excellent insertion and extraction kinetics of Li^+, favoring the transfer of electrons in the active component.

As for 0.2 C, with the increase of charging and discharging rates, the discharge capacities of microwave sintered and ordinary heated samples both decrease slightly, but they are still higher than 150 mAh g^{-1}. Although the voltage difference in the microwave sintered sample increases slightly (0.26 V) in comparison with the value tested at 0.1 C, it is much lower than that of the ordinary sintered sample (0.60 V). With regard to the microwave sintered sample, the discharge capacity is significantly mitigated, which is attributed to that microwave sintering inhibits grain growth, shortens the diffusion path of Li^+. This behavior improves the kinetics of Li^+ insertion and extraction as well as the transport properties of electrons in the bulk of the active material. Yu *et al.*[29] measured that the diffusion coefficient of the microwave sintered $LiFePO_4/C$ is 7.40×10^{-12} cm^2 s^{-1}, which is about two orders of magnitude higher than that of the ordinary sintered sample (3.68×10^{-14} cm^2 s^{-1}). Fig. 6C shows cyclic curves of $LiMn_{0.75}Fe_{0.25}PO_4/C$ composites at 0.1 C. One can observe that the capacities of the two samples are extremely close at the beginning of the cycles (about 152 mAh g^{-1}). Whereas the number of cycles increases, the degree of capacity decay becomes very different. The microwave sintered sample has an excellent cycle performance with a capacity of 143.5 mAh g^{-1} after 225 cycles, and the capacity retention rate is 94.3% as well as a very small capacity decay of only 0.04 mAh g^{-1} per cycle. However, the cycling performance of ordinary heating sintered samples has a severe capacity decay with only 24.7 % of capacity retention after 225 cycles. Especially, the capacity drops sharply after 100 cycles. The remarkable cycle performance of the microwave sintered sample is ascribed to the relatively small crystal grains, the uniform carbon coating on the surface and the conductive carbon network structure. The synergy effect allows the material particles to fully soak in the electrolyte, provides sufficient diffusion paths to Li^+ and inhibits dissolution of Mn. Moreover, the conductive carbon network structure can act as a buffer to alleviate the volume and structure changes during charge and discharge processes, thereby maintaining structural stability.

Fig. 6D shows the cyclic voltammetry (CV) curves of $LiMn_{0.75}Fe_{0.25}PO_4/C$ composites at the scanning speed of 0.1 mV s^{-1} over a voltage range of 2.5-4.5 V. There are two distinct reversible redox peaks corresponding to the valence transitions of Fe^{2+}/Fe^{3+} and Mn^{2+}/Mn^{3+} during Li^+ deintercalation and intercalation. The better the symmetry of the anodic/cathodic peaks on the curve, the higher the reversibility of Li^+ intercalation/deintercalation. For ordinary heating sintered sample, the cathodic peaks are at 3.78 and 4.53 V, the anodic peaks are at 3.20 and 3.57 V, and thus the potential differences are 0.58 and 0.96 V, respectively. Towards microwave sintered sample, the cathodic peaks are at 3.69 and 4.37 V, the anodic peaks are at 3.40 and 3.75 V, and thus the potential differences are 0.29 and 0.62 V, respectively, which are less than those of the ordinary heating sintered sample. The faster heating rate of the microwave sintering process leads to the sucrose pyrolysis at a molecular level and keeps a portion of carbon as a stereochemical net structure, which inhibits grain growth and results in the increment of electrical conductivity and thereby decreases electrode polarization. The impedance and the polarization phenomenon of the electrode produced by the microwave sintered sample are significantly reduced. Therefore, the electrode dynamic performance of the material is effectively improved.

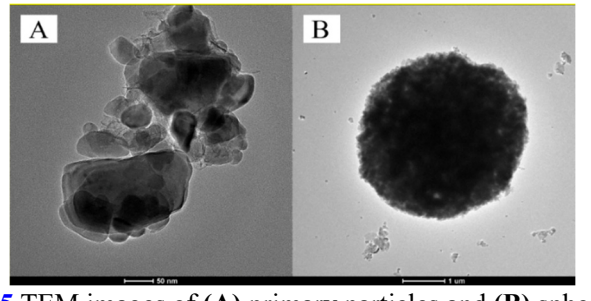

Fig. 5 TEM images of **(A)** primary particles and **(B)** spherical aggregate particles of $LiMn_{0.75}Fe_{0.25}PO_4/C$ composite calcined by microwave sintering.

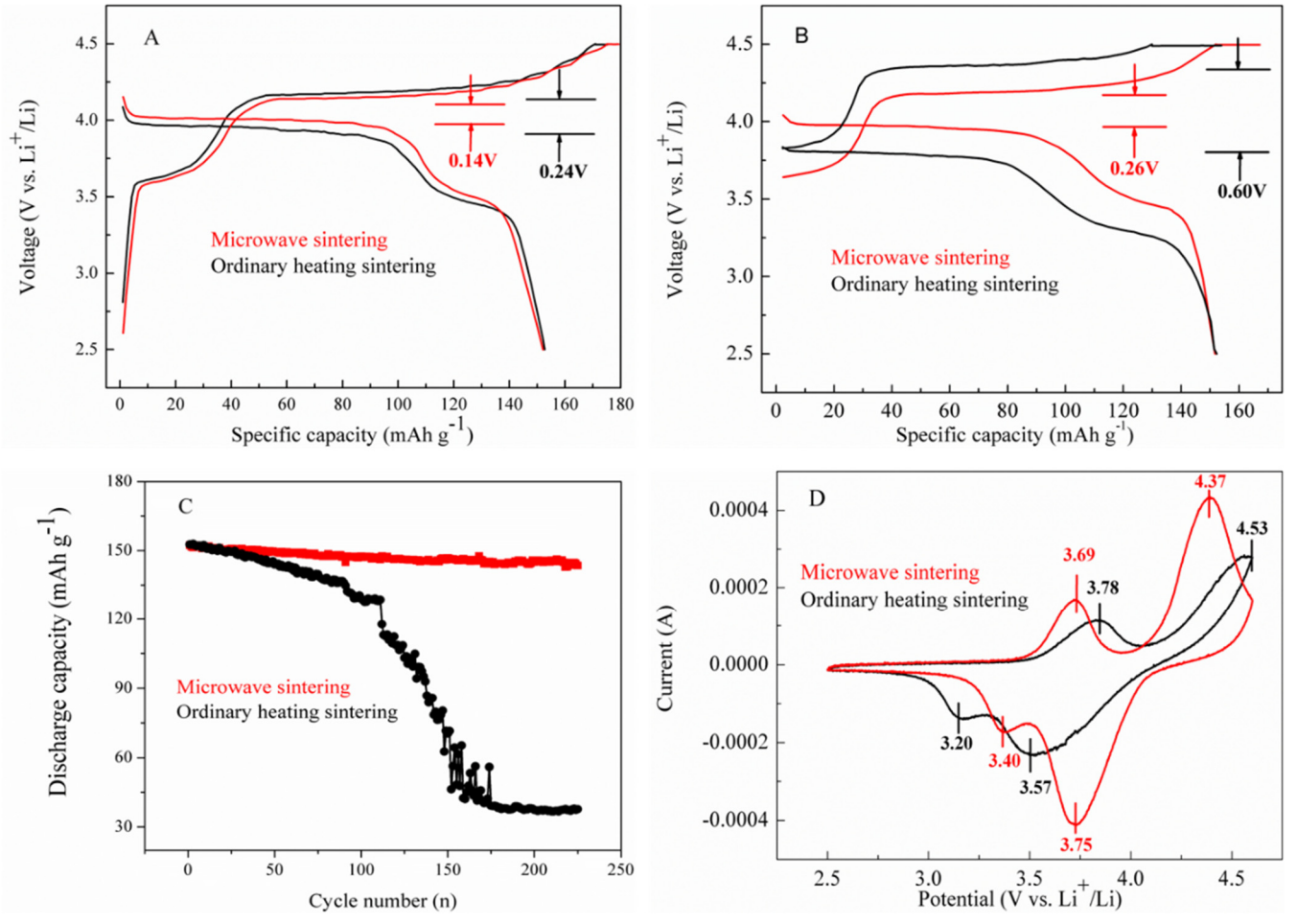

Fig. 6 Electrochemical properties of $LiMn_{0.75}Fe_{0.25}PO_4/C$ composites calcined by ordinary heating sintering and microwave sintering: charge-discharge curves at **(A)** 0.1 C and **(B)** 0.2 C, **(C)** cyclic curves, **(D)** cyclic voltammetry curves.

Fig. 7 shows the Nyquist plots of $LiMn_{0.75}Fe_{0.25}PO_4/C$ composites in the frequency range from 10^5 to 10^{-2} Hz. Both electrochemical impedance spectra consist of a depressed semicircle in the high-frequency region and a straight line in the low-frequency region. The numerical value of the diameter of the semicircle at high frequency on the Z_{re} axis is approximately the charge-transfer resistance (R_{ct}). The linear part at low frequency represents a typical Warburg behavior,[30] which is relative to the diffusion of Li^+ in the active cathode material. The value of the semicircular diameter of the microwave sintered electrode on the Z_{re} axis (172.58 Ω) is smaller than that of the ordinary heating sintered electrode (208.31 Ω), which means that the electrode material prepared by microwave sintering exhibits a lower R_{ct} and a higher conductivity and discharge capacity. The microwave sintering contributes to enhance the conductivity of the $LiMn_{0.75}Fe_{0.25}PO_4/C$ composite and reduce particle size, which renders the electron transfer and Li^+ intercalation/deintercalation much faster. Meanwhile, the formation of uniform carbon coating on the surface of particles and the structure of the conductive carbon network as well as the porous aggregate structure allows the active particles to be fully in touch with the electrolyte, thus improving the electrochemical dynamic properties of the electrode.

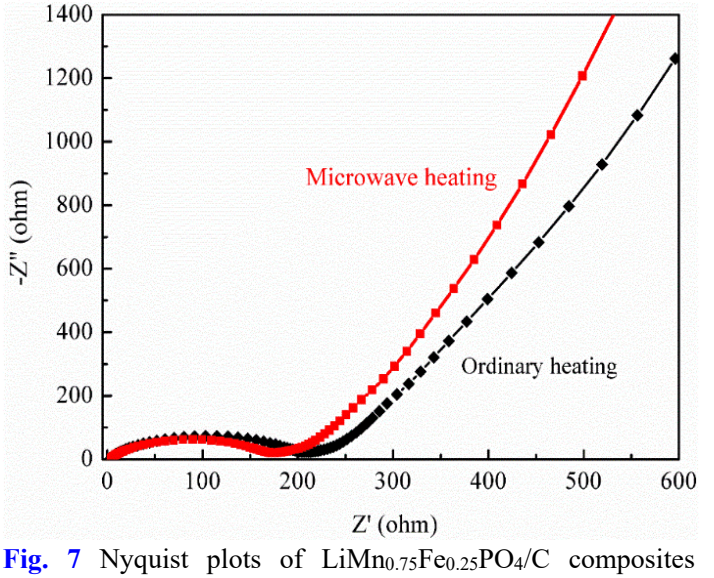

Fig. 7 Nyquist plots of $LiMn_{0.75}Fe_{0.25}PO_4/C$ composites calcined by ordinary heating sintering and microwave sintering in the frequency range 10^5 to 10^{-2} Hz.

4. Conclusions

In this paper, $LiMn_{0.75}Fe_{0.25}PO_4/C$ composites were prepared by the hydrothermal method assisted with ball milling, spray drying and microwave sintering. The influences of microwave sintering on the crystal structure and the electrochemical properties of $LiMn_{0.75}Fe_{0.25}PO_4/C$ composites were investigated in detail. It is found that the microwave sintering maintained a part of the carbon network structure and increased the porous structure and specific surface area of the material. Furthermore, microwave sintering contributed to reducing the grain size as well as the lattice parameters of $LiMn_{0.75}Fe_{0.25}PO_4/C$ composites from 299.66 $Å^3$ for ordinary heating sintering to 299.15 $Å^3$. Microwave sintering helped to form a uniform carbon coating layer on the surface of particles, the porous aggregate structure and the possible conductive carbon network structure, which enabled the material particles to fully contact the electrolyte, inhibited the dissolution of active Mn and improved the electrochemical kinetic properties of the material. The structure of the conductive carbon network provided a buffer carrier for the structure and volume changes during the Li^+ intercalation/deintercalation processes and maintained the structural stability. Compared to ordinary heating sintered sample, the microwave sintered sample presents an excellent electrochemical performance with a discharge capacity of 143.5 mAh g^{-1} and capacity retention of 94.3% at 0.1 C rate after 225 cycles, minor impedance and polarization, as well as improved electrode kinetics. This study demonstrates that the microwave sintering is an economic, energy-saving, and time-saving synthetic method for preparing electrode materials for high-performance batteries.

Acknowledgments

The authors would like to acknowledge the financial support from Key Research Project of North Minzu University (grant 2019KJ08), the Science and Technology Innovation Leader Program of Ningxia Hui Autonomous Region (grant KJT2015001), the Key Research Project of Ningxia Hui Autonomous Region (2016), the Program for Excellent Talents of Ningxia (grant 2018BEB04014), the Shandong Provincial Natural Science Foundation (grant ZR2019BB063), and the Applied Basic Research Foundation of Qingdao City (grant 19-6-2-13-cg).

Conflict of Interest

There is no conflict of interest.

Supporting Information

Not Applicable.

References

[1] A. K. Padhi, K. S. Nanjundaswamy and J. B. Goodenough, *J. Electrochem. Soc.*, 1997, **144**, 1188-1194, doi: 10.1149/1.1837571.

[2] F. Yu, L. Zhang, L. Lai, M. Zhu, Y. Guo, L. Xia, P. Qi, G. Wang and B. Dai, *Electrochim. Acta*, 2015, **151**, 240-248, doi: 10.1016/j.electacta.2014.11.014.

[3] J. Lim, Y. Li, D. H. Alsem, H. So, S. C. Lee, P. Bai, D. A. Cogswell, X. Liu, N. Jin, Y. S. Yu, N. J. Salmon, D. A. Shapiro, M. Z. Bazant, T. Tyliszczak and W. C. Chueh, *Science,* 2016, **353**, 566-571, doi: 10.1126/science.aaf4914.

[4] S. Choi, T. W. Kwon, A. Coskun and J. W. Choi, *Science,* 2017, **357**, 279-283, doi: 10.1126/science.aal4373.

[5] Y. Ma, C. Hou, H. Zhang, Q. Zhang, H. Liu, S. Wu and Z. Guo, *Electrochim. Acta,* 2019, **315**, 114-123, doi: 10.1016/j.polymer.2017.04.010.

[6] X. Jia, Y. Ma, Y. Liu, Y. Wang and Q. Zhang, *Catal. Lett.,* 2019, **149**, 2873-2886, doi: 10.1007/s10562-019-02823-6.

[7] Y. Wang, N. Li, C. Hou, B. He, J. Li, F. Dang, J. Wang and Y. Fan, *Ceram. Int.,* 2020, **46**, 9119-9128, doi: 10.1016/j.ceramint.2019.12.161.

[8] X. Zhang, X. Li, F. Jiang, W. Du, C. Hou, Z. Xu, L. Zhu, Z. Wang, H. Liu, W. Zhou and H. Yuan, *Dalton Trans.,* 2020, **49**, 1794-1802, doi: 10.1039/C9DT03845K.

[9] C. Hou, Y. Oaki, E. Hosono, H. Lin, H. Imai, Y. Fan and F. Dang, *Mater. Des.,* 2016, **109**, 718-725, doi: 10.1016/j.matdes.2016.07.099.

[10] M. Ma, Y. Yang, Y. Liu, W. Li, G. Chen, Y. Ma, P. Lyu, S. Li, Y. Wang and G. Wu, *Appl. Organomet. Chem.,* 2019, **33**, e4850, doi: 10.1002/aoc.4850.

[11] J. Yoshida, M. Stark, J. Holzbock, N. Hüsing, S. Nakanishi, H. Iba, H. Abe and M. Naito, *J. Power Sources,* 2013, **226**, 122-126, doi: 10.1016/j.jpowsour.2012.09.081.

[12] Z. Tan, X. Wang and H. Zhou, *Electrochim. Acta,* 2013, **90**, 597-603, doi: 10.1016/j.electacta.2012.12.027.

[13] S. M. Oh, S. W. Oh, C. S. Yoon, B. Scrosati, K. Amine and Y. K. Sun, *Adv. Funct. Mater.,* 2010, **20**, 3260-3265, doi: 10.1002/adfm.201000469.

[14] M. Zhao, Y. Fu, N. Xu, G. Li, M. Wu and X. Gao, *J. Mater. Chem. A,* 2014, **2**, 15070-15077, doi: 10.1039/c4ta03311f.

[15] W. Yang, Y. Bi, Y. Qin, Y. Liu, X. Zhang, B. Yang, Q. Wu, D. Wang and S. Shi, *J. Power Sources,* 2015, **275**, 785-791, doi: 10.1016/j.jpowsour.2014.11.063.

[16] J. Zheng, C. Qin, T. Wu, S. Xie, L. Ni, M. Peng, Y. Tang and Y. Chen, *J. Mater. Chem. A,* 2015, **3**, 15299-15306, doi: 10.1039/c5ta02431e.

[17] Y. Dong, L. Wang, S. Zhang, Y. Zhao, J. Zhou, H. Xie and J. B. Goodenough, *J. Power Sources,* 2012, **215**, 116-121, doi: 10.1016/j.jpowsour.2012.03.077.

[18] G. Li, H. Azuma and M. Tohda, *Electrochem. Solid-State Lett.,* 2002, **5**, A135-A137, doi: 10.1149/1.1475195.

[19] A. Paolella, G. Bertoni, E. Dilena, S. Marras, A. Ansaldo, L. Manna and C. George, *Nano Lett.,* 2014, **14**, 1477-1483, doi: 10.1021/nl4046697.

[20] J. K. Kim, R. Vijaya, L. Zhu and Y. Kim, *J. Power Sources,* 2015, **275**, 106-110, doi: 10.1016/j.jpowsour.2014.11.028.

[21] Y. Ma, M. Ma, X. Yin, Q. Shao, N. Lu, Y. Feng, Y. Lu, E. K. Wujcik, X. Mai, C. Wang and Z. Guo, *Polymer,* 2018, **156**, 128-135, doi: 10.1016/j.polymer.2018.09.051.
[22] Y. Ma, Z. Zhuang, M. Ma, Y. Yang, W. Li, M. Dong, S. Wu, T. Ding and Z. Guo, *Polymer,* 2019, **182**, 121808, doi: 10.1016/j.polymer.2019.121808.
[23] Y. P. Huang, T. Tao, Z. Chen, W. Han, Y. Wu, C. Kuang, S. Zhou and Y. Chen, *J. Mater. Chem. A,* 2014, **2**, 18831-18837, doi: 10.1039/C4TA03994G.
[24] C. Hou, Y. Ma, H. Zhang, W. Geng and Q. Zhang, *Mater. Technol.,* 2018, **33**, 16-21, doi: 10.1080/10667857.2017.1373488.
[25] J. Ni, Y. Han, L. Gao and L. Lu, *Electrochem. Commun.,* 2013, **31**, 84-87, doi: 10.1016/j.elecom.2013.03.022.
[26] J. Zong and X. Liu, *Electrochim. Acta,* 2014, **116**, 9-18, doi: 10.1016/j.electacta.2013.10.176.
[27] L. Hu, B. Qiu, Y. Xia, Z. Qin, L. Qin, X. Zhou and Z. Liu, *J. Power Sources,* 2014, **248**, 246-252, doi: 10.1016/j.jpowsour.2013.09.048.
[28] Y. T. Cui, N. Xu, L. Q. Kou, M. T. Wu and L. Chen, *J. Power Sources,* 2014, **249**, 42-47, doi: 10.1016/j.jpowsour.2013.10.036.
[29] B. Ding, G. Ji, Y. Ma, P. Xiao, L. Lu and J. Y. Lee, *J. Power Sources,* 2014, **247**, 273-279, doi: 10.1016/j.jpowsour.2013.08.114.
[30] Y. Ma, C. Hou, H. Zhang, M. Qiao, Y. Chen, H. Zhang, Q. Zhang and Z. Guo, *J. Mater. Chem. A,* 2017, **5**, 14041-14052, doi: 10.1039/c7ta03279j.
[31] S. Wang, F. Xie, X. Wu, Y. Ma, H. Du and G. Wu, *Ceram. Int.,* 2019, **45**, 18899-18907, doi: 10.1016/j.ceramint.2019.06.125.
[32] S. Liu, H. Fang, E. Dai, B. Yang, Y. Yao, W. Ma and Y. Dai, *Electrochim. Acta,* 2014, **116**, 97-102, doi: 10.1016/j.electacta.2013.11.052.
[33] B. Ding, P. Xiao, G. Ji, L. Lu and J. Y. Lee, *ACS Appl. Mater. Interfaces,* 2013, **5**, 12120-12126, doi: 10.1021/am403991f.
[34] L. Wu, S. Zhong, F. Lv and J. Liu, *Mater. Lett.,* 2013, **110**, 38-41, doi: 10.1016/j.matlet.2013.07.112.
[35] M. S. Kim, J. P. Jegal, K. C. Roh and K. B. Kim, *J. Mater. Chem. A,* 2014, **2**, 10607-10613, doi: 10.1039/c4ta01197j.
[36] F. Yu, S. H. Lim, Y. Zhen, Y. An and J. Lin, *J. Power Sources,* 2014, **271**, 223-230, doi: 10.1016/j.jpowsour.2014.08.009.
[37] C. Hou, Y. Hou, Y. Fan, Y. Zhai, Y. Wang, Z. Sun, R. Fan, F. Dang and J. Wang, *J. Mater. Chem. A,* 2018, **6**, 6967-6976, doi: 10.1039/c8ta00975a.
[38] C. Hou, J. Wang, W. Du, J. Wang, Y. Du, C. Liu, J. Zhang, H. Hou, F. Dang, L. Zhao and Z. Guo, *J. Mater. Chem. A,* 2019, **7**, 13460-13472, doi: 10.1039/c9ta03551f.
[39] C. Hou, Z. Tai, L. Zhao, Y. Zhai, Y. Hou, Y. Fan, F. Dang, J. Wang and H. Liu, *J. Mater. Chem. A,* 2018, **6**, 9723-9736, doi: 10.1039/c8ta02863j.

Publisher's Note

Engineered Science Publisher remains neutral with regard to jurisdictional claims in published maps and institutional affiliations.